ACTIVE-ARRAY BEAMFORMING FOR ULTRA-WIDEBAND IMPULSE RADAR

Malek G. M. Hussain, Kuwait University, Al-Khaldiah, State of Kuwait
Matthew J. Yedlin, University of British Columbia, Vancouver, BC, Canada

Abstract

Ultra-wideband electromagnetic impulses have found numerous applications for radar and radio communications due to the recent technological advances in electronic and opto-electronic devices. This paper presents the principle of active-array beamforming for ultra-wideband impulse radar. The theory and analysis are based on a realizable signal model representing the impulse-type waveforms used in radar applications. The signal model is referred to as the *generalized Gaussian* pulse. Impulse waveforms radiated and received by an active-array beamforming system suffer a directional distortion that can be regarded as useful information for direction finding and automatic beam steering. The directional distortion associated with the energy density spectrum of the generalized Gaussain pulse is derived and plotted for different values of the angle of incidence. Also, the directivity pattern of the array beamforming system is expressed in terms of the energy of the radiated and received impulse waveforms. Computer plots of the sidelobe-free directivity-energy pattern are presented too. The energy pattern yields high angular-resolution capability that improves by inceasing the spatial frequency bandwidth. The spatial frequency bandwidth is an important design parameter that allows a trade-off between effective bandwidth and array length for achieving a small resolution angle.

Introduction

The last decade of the 20th century marks the evolution of ultra-wideband (UWB) radar technology and its numerous applications for the military and the civil sectors. The rapid technological advances in the fields of solid-state electronic and opto-electronic (switching) devices, high-energy (microwave) sources, and super-fast digital computers are promising cost-effective UWB radar systems for the new millennium.

A subclass of UWB radar systems is the impulse radar. The waveform of impulse radar is a carrier-free pulse (or a coded sequence of pulses) occupying a large-relative bandwidth $\eta \approx 1$. The relative bandwidth $\eta = (f_H - f_L)/(f_H + f_L)$, where f_H and f_L are the highest and the lowest frequency components of the signal spectrum. The combined features of low-frequency content and the ultra-wide bandwidth of impulse-type waveforms make them very attractive for the use in many civil and military radar applications where the conventional radar systems are almost obsolete [1]–[5]. Due to the inherent low-energy content of electromagnetic impulses, the capabilities of impulse radar are limited to short-range applications. An active-array-antenna system with high-energy sources, and super-fast switching devices, is an efficient solution for enhancing the target-detection and resolution capabilities of impulse radar.

The principle of array beamforming based on carrier-free siganls introduced in the literature [6], [7] is based on nonsinusoidal radar signals with the time variation of rectangular and Gaussian pulses. These pulses have practical restrictions from the radiation point of view. The energy spectrum of ideal rectangular and Gaussian pulses includes a dc component, and consequently, they cannot be radiated by any type of antenna.

In this paper, we present the principle of active-array beamforming based on a realizable UWB carrier-free signal having an energy density spectrum free from a dc component. The signal model, its autocorrelation function and energy spectrum are introduced. The directional distortion associated with the spectrum of the radiated and received impulse waveforms will be derived for the active array beamforming system. The directional distortion can be regarded as valuable information for automatic beam steering and target tracking. Also, the directivity energy pattern of impulse waveforms is derived and plotted for different design parameters. The energy pattern of impulse waveforms is free from sidelobes and includes a mainlobe with a narrow beam width that is inversely proportional to frequency bandwidth and array length. These features are attractive for achieving high-angular resolution and for radar imaging [4].

Signal Model for Impulse Waveforms

Carrier-free electromagnetic signals radiated by an impulse antenna can analytically be represented by the time function [7]

$$\begin{aligned}\Omega(t) &= \frac{E_\circ}{1-\alpha}\left(\exp\{-\pi[(t-t_\circ)/\Delta T]^2\}\right. \\ &- \left.\alpha\exp\{-\pi[\alpha(t-t_\circ)/\Delta T]^2\}\right), \qquad (1)\end{aligned}$$

where $E_\circ$ is the peak amplitude at the time $t = t_\circ$, ΔT is the effective duration, and α is a scaling factor. We refer to the time function $\Omega(t)$ as the generalized Gaussain (GG) pulse. The autocorrelation function $\Upsilon(t)$ of the GG pulse

is given by,

$$\Upsilon(t) = \int_{-\infty}^{+\infty} \Omega(\lambda)\Omega(\lambda+t)\,d\lambda$$
$$= E_\circ^2 \Delta T \sum_{k=0}^{2} I_k \exp\{-a_k[(t-t_\circ)/\Delta T]^2\}, \quad (2)$$

where

$$I_0 = \frac{1}{\sqrt{2}(1-\alpha)^2}, \qquad a_0 = \frac{\pi}{2}, \quad (3)$$

$$I_1 = \frac{\alpha}{\sqrt{2}(1-\alpha)^2}, \qquad a_1 = \frac{\pi\alpha^2}{2}, \quad (4)$$

$$I_2 = \frac{-2\alpha}{(1-\alpha)^2(1+\alpha^2)^{1/2}}, \qquad a_2 = \frac{\pi\alpha^2}{(1+\alpha^2)}. \quad (5)$$

The Fourier transform of the GG pulse is

$$\Lambda(f) = \int_{-\infty}^{+\infty} \Omega(t)\exp\{-j2\pi ft\}\,dt$$
$$= \frac{E_\circ \exp\{-j2\pi t_\circ(f/\Delta f)\}}{\Delta f(1-\alpha)}\left[\exp\{-\pi(f/\Delta f)^2\}\right.$$
$$- \left.\exp\{-(\pi/\alpha^2)(f/\Delta f)^2\}\right], \quad (6)$$

where $\Delta f = 1/\Delta T$ is the effective frequency bandwidth of the GG pulse. The time variation of the normalized GG pulse $\Omega(t)/E_\circ$, the normalized autocorrelation function $\Upsilon(t)/\Upsilon(0)$, and the energy density spectrum $\Psi(f) = |\Lambda(f)|^2$ are shown in Fig. 1 for the values of the scaling factor $\alpha = 0$ (dotted line), $\alpha = 0.3$ (dashed line), $\alpha = 0.6$ (dashed-dotted line), and $\alpha = 1.2$ (solid line). For $\alpha = 0$, $\Omega(t)$ is an ideal Gaussian pulse and its energy density spectrum in Fig. 1c (dotted line) includes a dc component at the normalized frequency $f/\Delta f = 0$. The GG pulse is a convenient signal model for developing the theory and analysis of impulse radar and communications.

Impulse-Array Beamforming

An active array beamforming system for UWB impulse radar is shown in Fig. 2. The $2m+1$ equally spaced array elements have dual role as radiators and as sensors for emitting and receiving electromagnetic impulses. The transmitter module includes pulse generators and driving circuits (PG-DC$_i$), $i = 0, \pm1, \pm2, \ldots, \pm m$, for switching and delivering high peak-power transient currents to the array elements. Each array element is also connected to the receiver module via a duplexer, which isolates the receiver during the transmitting mode of the antenna array system. The receiver module is a beam forming network consisting of $2m+1$ sliding correlators (SC$_i$), Fourier transform processors (FTP$_i$), and a summer circuit (SUM). Proper shielding is necessary for all the equipment in the transmitter and the receiver modules for protection against mutual coupling.

Let the GG pulse $\Omega(t)$ given in (1) be radiated by the array elements in Fig. 2. A point scatterer in the far field at an angle ϕ with respect to the array axis reflects back to the antenna array a waveform having the time variation

$$\Omega_T(t,\phi) = \sum_{i=-m}^{+m} \Omega(t-\tau_i(\phi)), \quad (7)$$

where the normalized propagation delay

$$\tau_i(\phi)/\Delta T = (id/c\Delta T)\sin\phi$$
$$= (i/2m)\rho\sin\phi, \quad (8)$$

and

$$\rho = 2md/c\Delta T = L/c\Delta T = L\Delta f/c. \quad (9)$$

In (8) and (9), ρ is referred to as the *spatial frequency bandwidth*, d is the separation distance between adjacent array elements, and $L = 2md$ is the array length. For antenna array with a large number of elements, $m \gg 1$, the summation in (7) can be approximated by an integral with the help of the following substitutions: $\eta = i/2m, d\eta = d(i/2m)$, and for $i - \pm m \to -1/2 \le \eta \le +1/2$. The integral form of $\Omega_T(t,\phi)$ is expressed as follows,

$$\Omega_T(t,\phi) \approx 2m\int_{-1/2}^{+1/2} \Omega(t-\eta\rho\sin\phi)\,d\eta \quad (10)$$

With the help of (6), the Fourier transform of $\Omega_T(t,\phi)$ results in the amplitude-spectral-density function

$$\Lambda_T(f,\phi) = 2m\Lambda(f)\frac{\sin[\pi\rho(f/\Delta f)\sin\phi]}{\pi\rho(f/\Delta f)\sin\phi}$$
$$= 2m\Lambda(f)\mathrm{sinc}[\pi\rho(f/\Delta f)\sin\phi]. \quad (11)$$

During the receiving mode of the beamforming system in Fig. 2, the arriving wavefront is transduced by the array elements into voltage signals with the time variation $\Omega_T(t-\tau_i(\phi)), i = 0, \pm1, \pm2, \ldots, \pm m$. Each voltage signal is passed through the SC$_i$ to be correlated by a replica of the radiated GG pulse $\Omega(t)$. The correlation process yields maximum signal-to-noise ratio for the case of additive white Gaussian noise. The voltage signal from the SC$_i$ is then transformed into the frequency domain by the FTP$_i$ to result in the energy density spectrum of the received signal. This transformation is convenient for *space-frequency* analysis of impulse waveforms formulated at the output of the beamforming system.

In principle, each sliding correlator SC$_i$ in Fig. 2 can be regarded as a matched filter having a transfer function $\Lambda^*(f)$, where the asterisk denotes complex conjugate. In analogy to (7) and (11), the energy-spectral-density function at the output of SUM in Fig. 2 can be expressed as follows,

$$\Psi_T(f,\phi) = \Lambda(f)\Lambda^*(f)\{2m\mathrm{sinc}[\pi\rho(f/\Delta f)\sin\phi]\}^2$$
$$= \Psi(f)\left[H_A(f,\phi)\right]^2 \quad (12)$$

In (12), $\Psi(f) = |\Lambda(f)|^2 = \Lambda(f)\Lambda^*(f)$ is the energy density spectrum of the radiated GG pulse, and

$$H_A(f,\phi) = 2m\text{sinc}[\pi\rho(f/\Delta f)\sin\phi] \qquad (13)$$

is the transfer function of the array beamforming system in Fig. 2. In the case of a complex target that is composed of a finite number of scattering centers, and having a transfer function $H_T(f,\phi)$, the spectrum of the received signal at the output of SUM in the array system of Fig. 2 can be expressed as follows,

$$\widetilde{\Psi}_T(f,\phi) = \Psi(f)H_T(f,\phi)\left[H_A(f,\phi)\right]^2. \qquad (14)$$

The energy-spectral-density function $\Psi_T(f,\phi)$ given in (12) is plotted in Fig. 3 as a function of normalized frequency $f/\Delta f$, for the values of $\alpha = 0.5$, $\rho = 100$, and the angle of incidence (a) $\phi = 0°$, (b) $\phi = 2°$, (c) $\phi = 4°$, and (d) $\phi = 8°$. For on axis reception, $\phi = 0°$, the energy spectrum $\Psi_T(f,0) = \Psi(f)$. For off-axis reception, $\phi > 0°$, the energy spectrum $\Psi_T(f,\phi)$ at the output of SUM in Fig. 2 is a distorted (or modulated) version of the radiated energy spectrum $\Psi(f)$. The different modulation patterns, or directional distortions, shown in Fig. 3 can be regarded as useful information for direction finding and electronic beam steering. According to Fig. 3, the frequency of oscillation in the modulated spectrum $\Psi_T(f,\phi)$ is an increasing function of the angle ϕ. Hence, a measure of the frequency of oscillation results in an estimate, $\hat{\phi}$, of the angle of incidence ϕ. This estimate can then be used to calculate the required delay time for each array element so that a main beam can electronically be steered into the direction of the signal source, as in the case of *retro-directive array systems*.

The beamforming system in Fig. 2 can be advanced to operate as a retro-directive array system by employing a variable delay circuit (VDC_i) at each array element, and having them controlled by a delay adjustment computer (DAC). The output signal of SUM will be passed to the DAC to calculate the estimate $\hat{\phi}$ and adjust, accordingly, the delay of each VDC_i to achieve beam steering.

Directivity Energy Pattern

For impulse waveforms, the directivity energy pattern $W(\phi)$ of the beamforming system in Fig. 2 can be defined in terms of the ratio

$$W(\phi) = U(\phi)/U(0), \qquad (15)$$

where

$$U(\phi) = \int_0^\infty (|\Lambda(f)|\text{sinc}[\pi\rho(f/\Delta f)\sin\phi])^2\, df \qquad (16)$$

is the energy of the received signal at the output of SUM, and

$$U(0) = \int_0^\infty |\Lambda(f)|^2\, df, \qquad (17)$$

The energy pattern $W(\phi)$ is plotted in Fig. 4 for the values of $\alpha = 0.5$, and $\rho = 10$ (dotted line), $\rho = 20$ (dashed line), $\rho = 30$ (dashed-dotted line), and $\rho = 40$ (solid line). The half-energy-point beamwidth of $W(\phi)$, which defines the resolution angle, is narrower for the larger values of the spatial frequency bandwidth ρ. Hence, the resolution angle, ε, for the energy pattern $W(\phi)$ is inversely proportional to ρ, and can be expressed as follows,

$$\varepsilon = K/\rho = Kc/L\Delta f. \qquad (18)$$

where c is speed of light, and K proportionality constant. The trade-off between effective bandwidth Δf and array length L for a small resolution angle ε is attractive in practice, especially, for the applications where signal attenuation due to the propagation media is severe for the higher frequencies [4].

Conclusions

Impulse-type waveforms used for UWB radar applications can analytically be represented by a gneralized Gaussain pulse having a realizable energy density spectrum. Active-array beamforming based on impulse waveforms yields directional distortion in the energy spectrum of the received and combined signals. The directional distortion of impulse waveforms is a useful feature for automatic beam steering. The directivity energy pattern of impulse-array systems is characterized by a narrow mainlobe and no sidelobes. The half-energy beamwidth of the directivity pattern defines the resolution angle as a decreasing function of the effective bandwidth and the array length. Such a relationship is attractive in practice, especially, for high-resolution imaging radar.

References

[1] Harmuth, Henning F., Raouf N. Boules, and Malek G.M. Hussain (1999), *Electromagnetic Signals:Reflection, Focusing, Distortion, and their Practical Applications.* New York: Kluwer Academic/Plenum.

[2] Taylor, James D. (Editor) (1995), *Introduction to Ultra–wideband Radar Systems.* Florida: CRC Press.

[3] Hussain, Malek G.M. (1998), "Ultra-wideband impulse radar—An overview of principles, *IEEE AES Magazine,* vol. 13, no. 9, pp. 9–14.

[4] Carin, Lawrence, Norbert Geng, Mark McClure, Jeffrey Sichina, and Lam Nguyen (1999), "Ultra-wideband synthetic-aperture radar for mine-field detection," *IEEE Antennas and Propagation Magazine,* vol. 41, no. 1, pp. 18–33.

[5] Win, Moe Z., and Robert A. Scholtz (1998), "Impulse Radio: How it works," *IEEE Communications Letter, vol. 2, no. 2, pp. 36–38.*

[6] Harmuth, Henning F. (1984), *Antennas and Waveguides for Nonsinusoidal Waves.* New York: Academic Press.

[7] Hussain, Malek G.M. (1988), "Antenna patterns of nonsinusoidal waves with the time variation of a Gaussian pulse—Part I", *IEEE Trans. Electromagn. Compat.*, vol. EMC-30, no. 4, pp. 504–512.

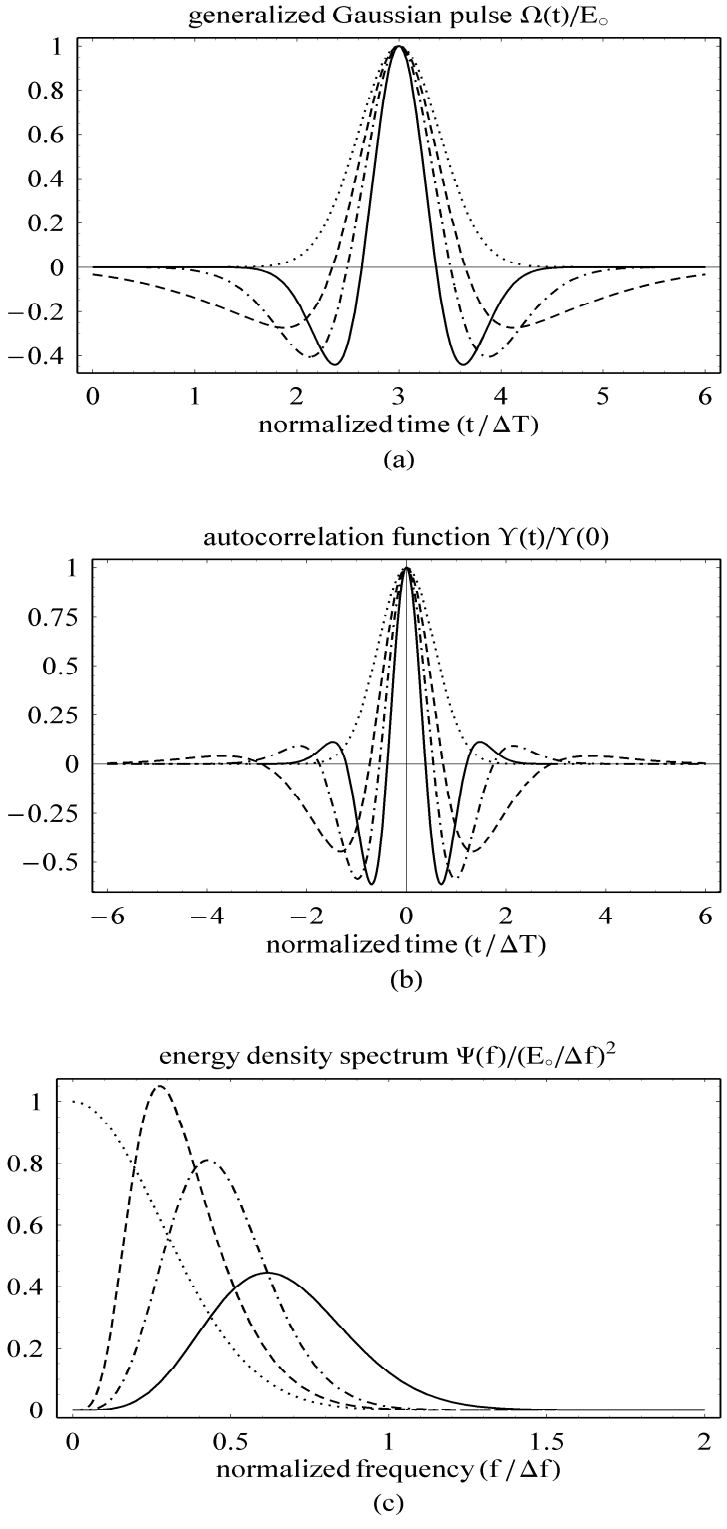

Figure 1. Normalized time variation of the generalized Gaussian pulse $\Omega(t)/E_\circ$ (a), autocorrelation function $\Upsilon(t)/\Upsilon(0)$ (b), and energy density spectrum $\Psi(f) = |\Lambda(f)|^2$ (c), for values of the scaling parameter $\alpha = 0$ (dotted line), $\alpha = 0.3$ (dashed line), $\alpha = 0.6$ (dashed-dotted line), and $\alpha = 1.2$ (solid line).

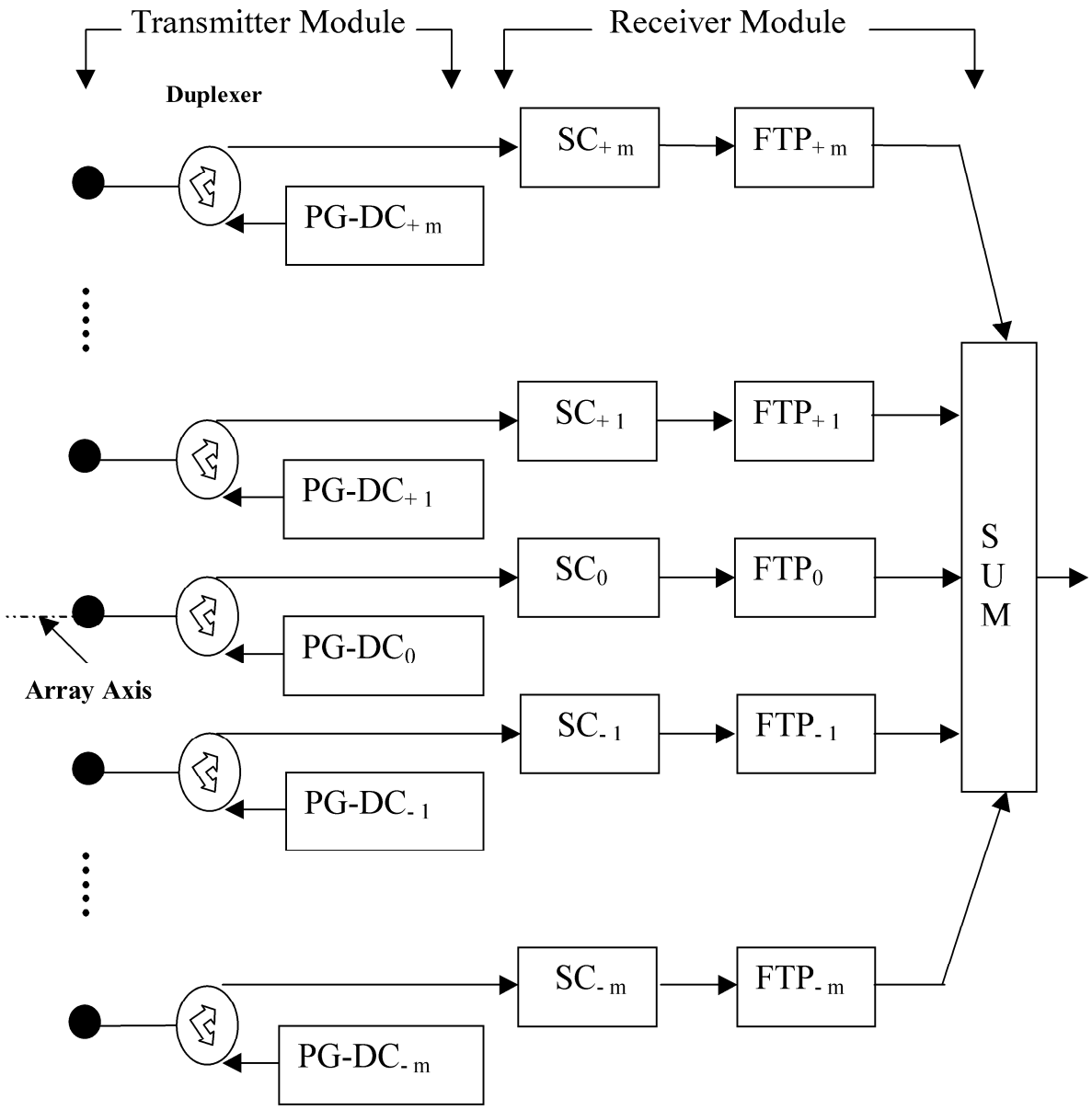

Figure 2. Active array beamforming system for UWB impulse radar. Each one of the $2m+1$ array elemnts is connected to a duplexer, pulse generator and driving circuits (PG-DC$_i$), sliding correlator (SC$_i$), Fourier transform processor (FTP$_i$), and summer circuit (SUM).

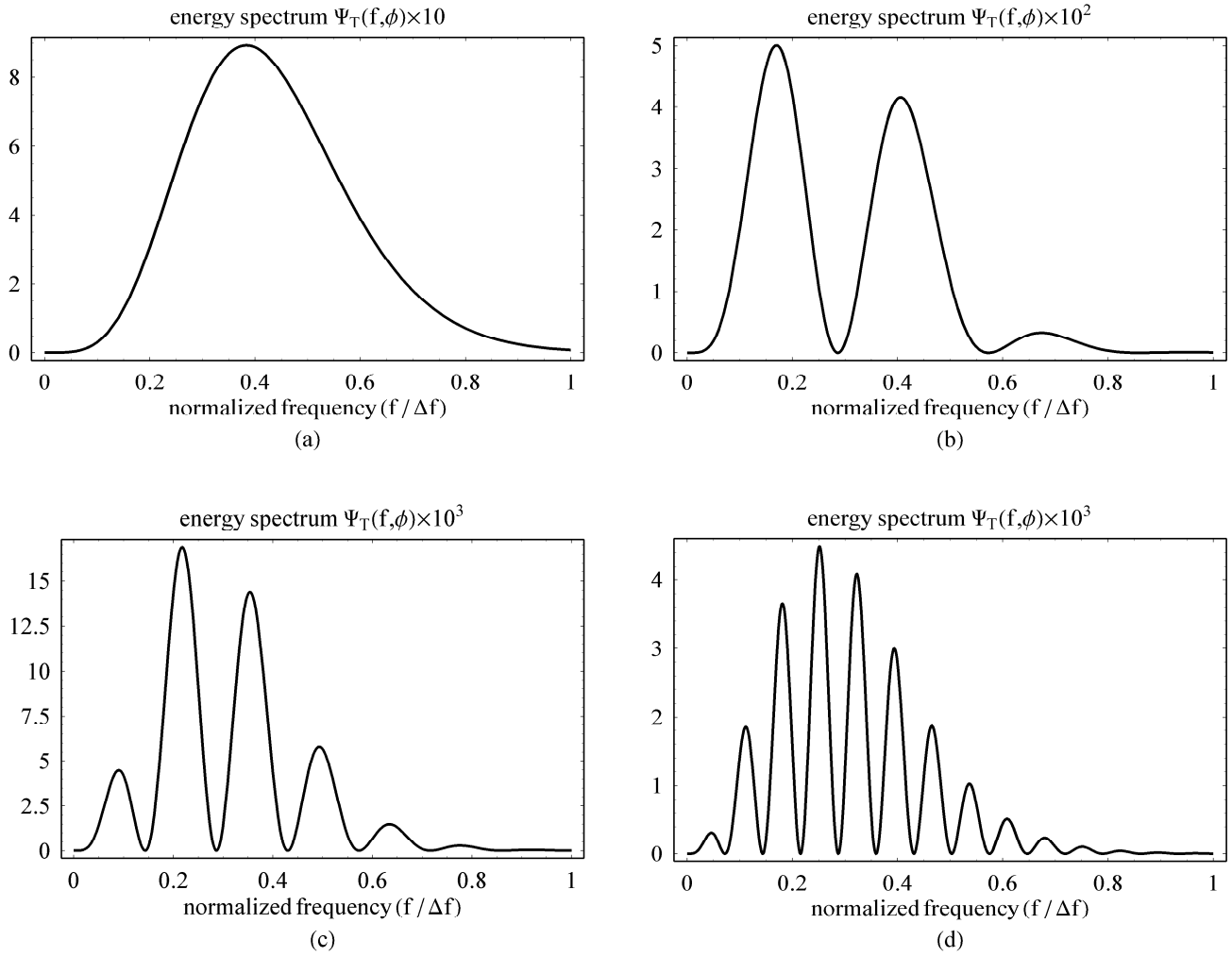

Figure 3. Energy density spectrum $\Psi_T(f,\phi)$ at the output of the beamforming system in Fig. 2 for $\alpha = 0.5$, $\rho = 100$, and the angle of incidence (a) $\phi = 0°$, (b) $\phi = 2°$, (c) $\phi = 4°$, and (d) $\phi = 8°$.

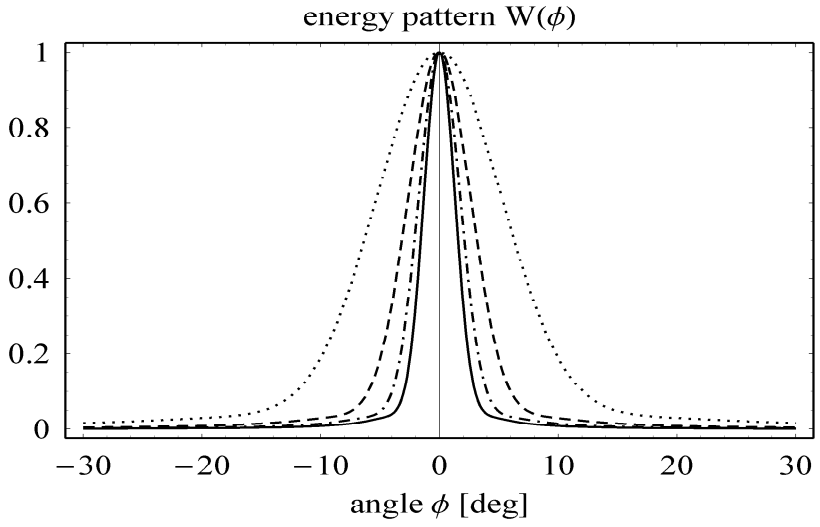

Figure 4. Directivity energy pattern $W(\phi)$ for the scaling parameter $\alpha = 0.5$, and the values of the spatial frequency bandwidth $\rho = 10$ (dotted line), 20 (dashed line), 30 (dashed-dotted line), and 40 (solid line).